DNA nanoparticle-mediated *ABCA4* delivery rescues Stargardt dystrophy in mice

Zongchao Han,[1] Shannon M. Conley,[1] Rasha S. Makkia,[1] Mark J. Cooper,[2] and Muna I. Naash[1]

[1]Department of Cell Biology, University of Oklahoma Health Sciences Center, Oklahoma City, Oklahoma, USA.
[2]Copernicus Therapeutics Inc., Cleveland, Ohio, USA.

Mutations in the photoreceptor-specific flippase *ABCA4* are associated with Stargardt disease and many other forms of retinal degeneration that currently lack curative therapies. Gene replacement is a logical strategy for *ABCA4*-associated disease, particularly given the current success of traditional viral-mediated gene delivery, such as with adeno-associated viral (AAV) vectors. However, the large size of the *ABCA4* cDNA (6.8 kbp) has hampered progress in the development of genetic treatments. Nonviral DNA nanoparticles (NPs) can accommodate large genes, unlike traditional viral vectors, which have capacity limitations. We utilized an optimized DNA NP technology to subretinally deliver *ABCA4* to *Abca4*-deficient mice. We detected persistent *ABCA4* transgene expression for up to 8 months after injection and found marked correction of functional and structural Stargardt phenotypes, such as improved recovery of dark adaptation and reduced lipofuscin granules. These data suggest that DNA NPs may be an excellent, clinically relevant gene delivery approach for genes too large for traditional viral vectors.

Introduction

Compacted DNA nanoparticles (NPs) (8–10 nm in diameter) formulated with polyethylene glycol-substituted polylysine (CK30PEG) are highly efficient in transfecting postmitotic cells (1–5), are biodegradable (3, 4), and exhibit minimal toxicity, even after repeated dosing, to the eye, lung, and brain (1, 2, 5–7). In contrast with many other nonviral approaches, these NPs drive long-term gene expression (1, 2) after subretinal delivery to the mouse eye, making them an excellent choice for chronic retinal degenerations such as Stargardt. They have recently been used to mediate phenotypic rescue in rodent models of retinitis pigmentosa, Parkinson disease, and cystic fibrosis, and were safely employed in a phase I/II clinical trial for cystic fibrosis (2, 8, 9). One distinguishing feature of these NPs is their large capacity. Studies using luciferase reporter vectors ranging in size from 5.3 to 20.2 kbp (generated by introducing λ-bacteriophage DNA fragments into the parent plasmid) demonstrated comparable gene expression regardless of vector size, suggesting that these NPs could deliver large genes (10).

Stargardt disease patients exhibit delayed dark adaptation and severe macular vision loss as well as characteristic fundus/histological changes including accumulation of lipofuscin granules in the retinal pigment epithelium (RPE), increased levels of the bisretinoid A2E in the RPE, and fundus flecking (11). Adeno-associated viral–based (AAV-based) gene therapy for *ABCA4* (ATP-binding cassette, subfamily A, member 4) has been attempted (12); however, subsequent reports demonstrated that the AAVs employed contained a heterogenous mix of DNA, not intact *ABCA4* expression cassettes (13). Lentivirus-based therapy for *ABCA4* gene delivery has also been used to attenuate A2E accumulation in *Abca4*$^{-/-}$ (14), and preliminary lentiviral clinical trials have recently begun (NCT01367444), but the need for effective therapies remains great.

Results and Discussion

Given the packaging capacity of our NPs, we evaluated whether they could express the large *ABCA4* therapeutic gene and mediate improvement in a Stargardt disease model (15). We constructed CK30PEG NP–carrying (4.3 mg DNA/ml) vectors (13–14 kbp) with the human *ABCA4* cDNA and the photoreceptor-specific human interphotoreceptor retinoid-binding protein (IRBP-ABCA4) promoter or the mouse opsin (MOP-ABCA4) promoter (1, 2) and confirmed that the NPs carried intact plasmid (Supplemental Figure 1; supplemental material available online with this article; doi:10.1172/JCI64833DS1). NPs carrying nonfunctional mutant *ABCA4* (K969M, ref. 16) served as controls.

Abca4$^{-/-}$ mice were subretinally injected (1 μl) in the temporal central region at P30. One eye was injected with WT NPs, while the contralateral eye was injected with mutant NPs (mu-NPs). Controls were uninjected or saline injected. Transgene mRNA levels were evaluated in whole eyes by quantitative RT-PCR (qRT-PCR) using primers that amplify human and murine *ABCA4*, and transcript levels were normalized to β-actin. IRBP- and MOP-ABCA4 NPs generated *ABCA4* expression at all time points tested (Figure 1A). NP expression peaked at 2 months post injection (PI) and was still detectable at 8 months PI. However, expression from uncompacted vectors was undetectable by 3 months PI, so they were not included in subsequent experiments. There was no significant difference in the amount of message from IRBP-ABCA4 and MOP-ABCA4 NPs at any time point. mRNA levels from eyes injected with mutant vectors were consistently lower than those in eyes injected with WT vectors (Figure 1A), although the differences were not statistically significant.

We next examined protein levels from treated animals; Western blots of retinal extracts were probed with antibodies against human/mouse ABCA4 (Figure 1B, 1–3 represent individual mice). Protein levels were normalized to β-actin and expressed as a percentage of untreated WT (*Abca4*$^{+/+}$, Figure 1C). IRBP-ABCA4 and MOP-ABCA4 NPs generated similar protein levels, approximately 25% of WT at 2 months PI and approximately 11% at 8 months PI (Figure 1C). No expression (mRNA or protein) was detected in uninjected *Abca4*$^{-/-}$ or saline-injected animals.

Conflict of interest: Mark Cooper is an employee of Copernicus Therapeutics Inc. and holds stock in the company.

Citation for this article: *J Clin Invest.* 2012;122(9):3221–3226. doi:10.1172/JCI64833.

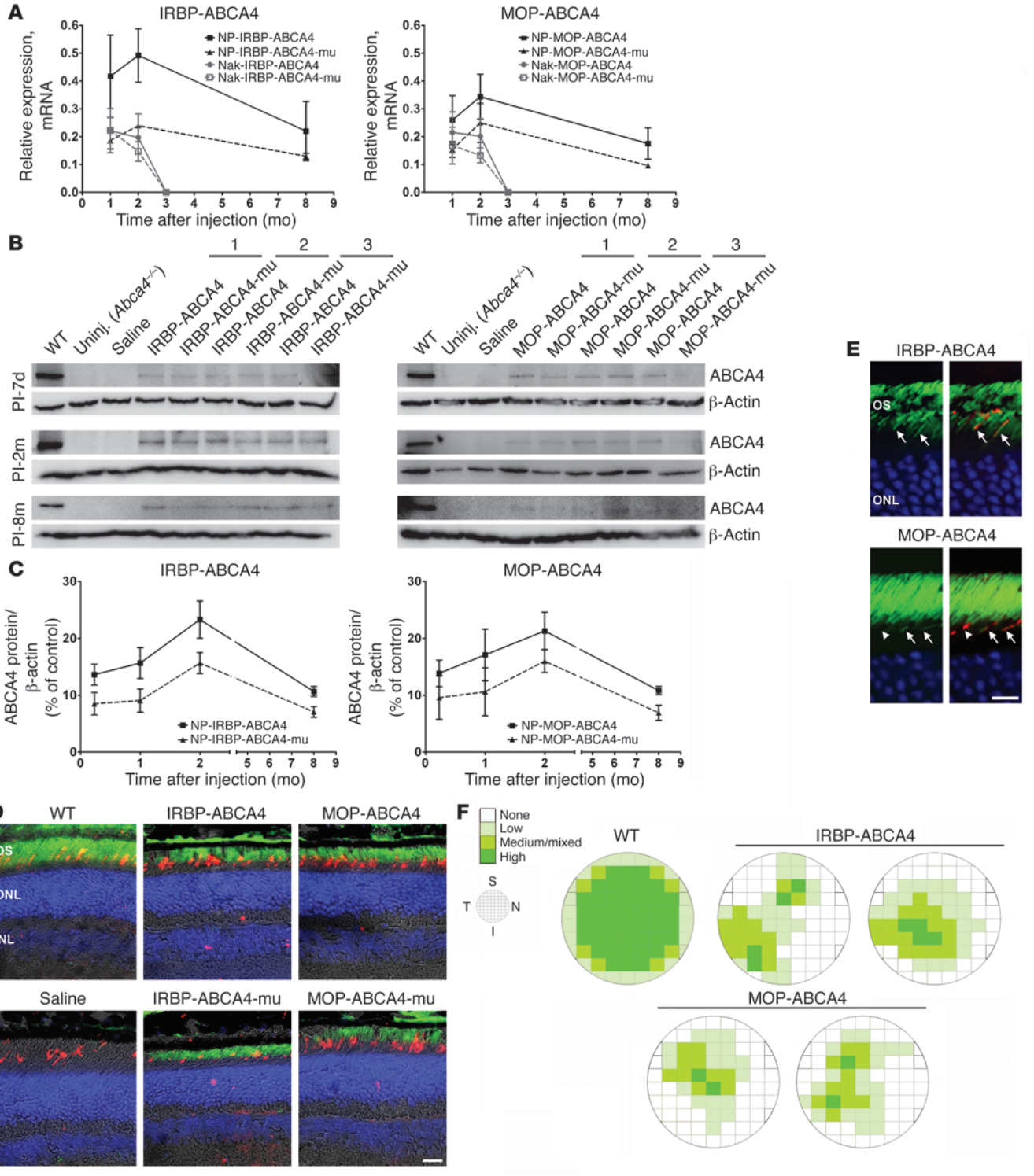
A
IRBP-ABCA4
MOP-ABCA4
Relative expression, mRNA
Time after injection (mo)
NP-IRBP-ABCA4
NP-IRBP-ABCA4-mu
Nak-IRBP-ABCA4
Nak-IRBP-ABCA4-mu
NP-MOP-ABCA4
NP-MOP-ABCA4-mu
Nak-MOP-ABCA4
Nak-MOP-ABCA4-mu
B
1
2
3
WT
Uninj. (Abca4−/−)
Saline
IRBP-ABCA4
IRBP-ABCA4-mu
MOP-ABCA4
MOP-ABCA4-mu
PI-7d
PI-2m
PI-8m
ABCA4
β-Actin
C
IRBP-ABCA4
MOP-ABCA4
ABCA4 protein/ β-actin (% of control)
Time after injection (mo)
NP-IRBP-ABCA4
NP-IRBP-ABCA4-mu
NP-MOP-ABCA4
NP-MOP-ABCA4-mu
D
WT
IRBP-ABCA4
MOP-ABCA4
Saline
IRBP-ABCA4-mu
MOP-ABCA4-mu
OS
ONL
INL
E
IRBP-ABCA4
MOP-ABCA4
OS
ONL
F
None
Low
Medium/mixed
High
S
T
N
I
WT
IRBP-ABCA4
MOP-ABCA4

Figure 1
NP-mediated *ABCA4* gene delivery induces persistent gene expression throughout the retina in *Abca4*$^{-/-}$ mice. (**A**) *ABCA4* mRNA levels were assessed by qRT-PCR and normalized to endogenous β-actin. Saline-injected and uninjected eyes were used as negative controls. (**B**) Western blots and quantitation thereof (**C**). Shown are 3 representative eyes at each time point/group (labels 1–3) injected with either WT or mutant NPs. (n = 4–6 eyes/group for **A**–**C**). Protein levels were normalized to β-actin and expressed as a percentage of levels found in uninjected WT mice. Results for WT and mu-NP treatment in **A** and **C** were analyzed by 2-way ANOVA with Bonferroni's post-hoc comparisons. (**D** and **E**) Retinal cryosections at 8 months PI were colabeled for ABCA4 (green), S-opsin (red) with DAPI (epifluorescent images/bright field, **D**; single planes of confocal stacks, **E**). Arrows, cones expressing ABCA4; arrowheads, cones not expressing ABCA4. (**F**) At 8 months PI, cryosections were collected approximately every 200 μm throughout the eye along the nasal-temporal plane and were labeled with antibodies against ABCA4 (green). In each section, adjacent ×40 fields (~200 μm across) were graded for level of expression by a blinded observer. Schematics depict distribution of transferred ABCA4 throughout the eye. Scale bars: 20 μm (**D**); 10 μm (**E**). OS, outer segment; INL, inner nuclear layer; S, superior; I, inferior; T, temporal; N, nasal.

To determine which retinal cells expressed the NPs, retinal sections at 8 months PI were labeled for ABCA4 (Figure 1, D and E) and short-wavelength cone opsin (Figure 1, D and E). Expression of ABCA4 was restricted to rod and cone outer segments (Figure 1D), consistent with the expression patterns of MOP and IRBP (refs. 1, 2, 17, and Figure 1E). To assess the panretinal distribution of NP-based expression at 8 months PI, images were collected from ABCA4-labeled sections throughout the eye (diagram in Supplemental Figure 2) and ABCA4 expression in each frame was graded as none, low, medium/mixed, or high. Schematics from these images demonstrated that expression is not restricted to the site of injection, but rather is distributed throughout the retina (Figure 1F). ABCA4 distribution is shown in Supplemental Figures 3–5. These results show that NPs drive long-term gene expression and promote transcription and translation of a large gene, both critical for treatment of chronic diseases such as Stargardt.

We next asked whether this expression improved the *Abca4*$^{-/-}$ phenotype. *Abca4*$^{-/-}$ mice (15) exhibit many of the clinical features associated with Stargardt, including fundus flecking (18), delayed dark adaptation, and accumulation of lipofuscin granules in the RPE (15). *Abca4*$^{-/-}$ mice initially exhibit abnormal white spots on the fundus at 3 months of age (18). Fundus images were obtained from NP-treated and control mice; as expected, at 1 month PI, none of the eyes showed white spots regardless of treatment (Figure 2A). In contrast, at 8 months PI, abnormal fundus spots were seen in uninjected, saline-injected (not shown), and IRBP-ABCA4-mu/MOP-ABCA4-mu NP–treated eyes but not WT or IRBP-ABCA4/MOP-ABCA4 NP–treated eyes (Figure 2B). Additional eyes are shown in Supplemental Figure 6.

To assess the ability of NPs to prevent the buildup of lipofuscin (Figure 3A), electron micrographs of the RPE were collected at 8 months PI in the temporal central region (Figure 3A). The number of lipofuscin granules/μm² of RPE was plotted (Figure 3B). As expected, we saw a statistically significant increase in lipofuscin granules in *Abca4*$^{-/-}$ compared with WT mice. In contrast, lipofuscin granules in MOP-ABCA4– and IRBP-ABCA4–injected eyes were significantly reduced compared with uninjected animals (Figure 3B). This reduction brought lipofuscin levels in NP-treated eyes almost back to WT levels; although means were higher in NP-treated animals than in WT, the difference was not statistically significant. Mutant NPs had no effect on lipofuscin accumulation compared with uninjected, confirming that the striking beneficial effects of IRBP-ABCA4 and MOP-ABCA4 were due not to the NPs per se, but rather to the NP-driven expression of functional ABCA4. We also observed the expected thickening of Bruch membrane (BrM) (Figure 3A) in *Abca4*$^{-/-}$ mice compared with WT. This thickening was attenuated (although without statistical significance) in eyes treated with IRBP-ABCA4 and MOP-ABCA4 NPs, but not mutant NPs (Figure 3C).

These RPE defects are thought to lead to the eventual degeneration of the photoreceptor cell layer (outer nuclear layer [ONL]) in Stargardt patients and *Abca4*$^{-/-}$ mice. Significant degeneration in *Abca4*$^{-/-}$ mice is detected by 8 months PI (19), so it is not surprising that we detected no changes in ONL morphometry at

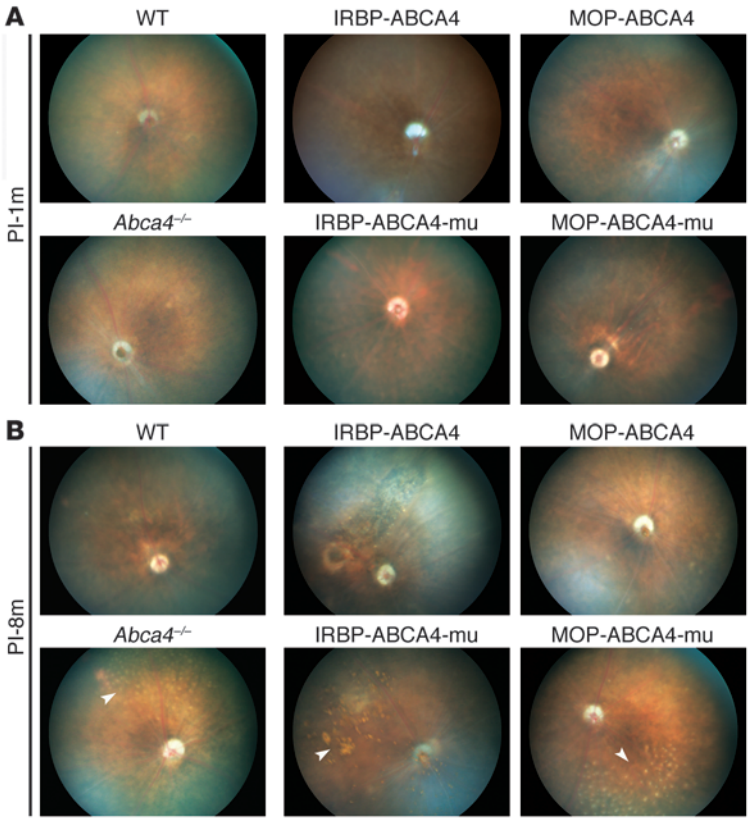

Figure 2
NP-mediated *ABCA4* gene delivery reduces retinal flecking in *Abca4*$^{-/-}$ mice. Shown are representative in vivo fundus images captured from treated *Abca4*$^{-/-}$ mice at 1 month PI (**A**) and 8 months PI (**B**). Age-matched WT and uninjected *Abca4*$^{-/-}$ mice were used as controls. White arrowheads show retinal flecking in uninjected and mutant-construct–injected animals but not WT or IRBP-ABCA4/MOP-ABCA4–treated animals.

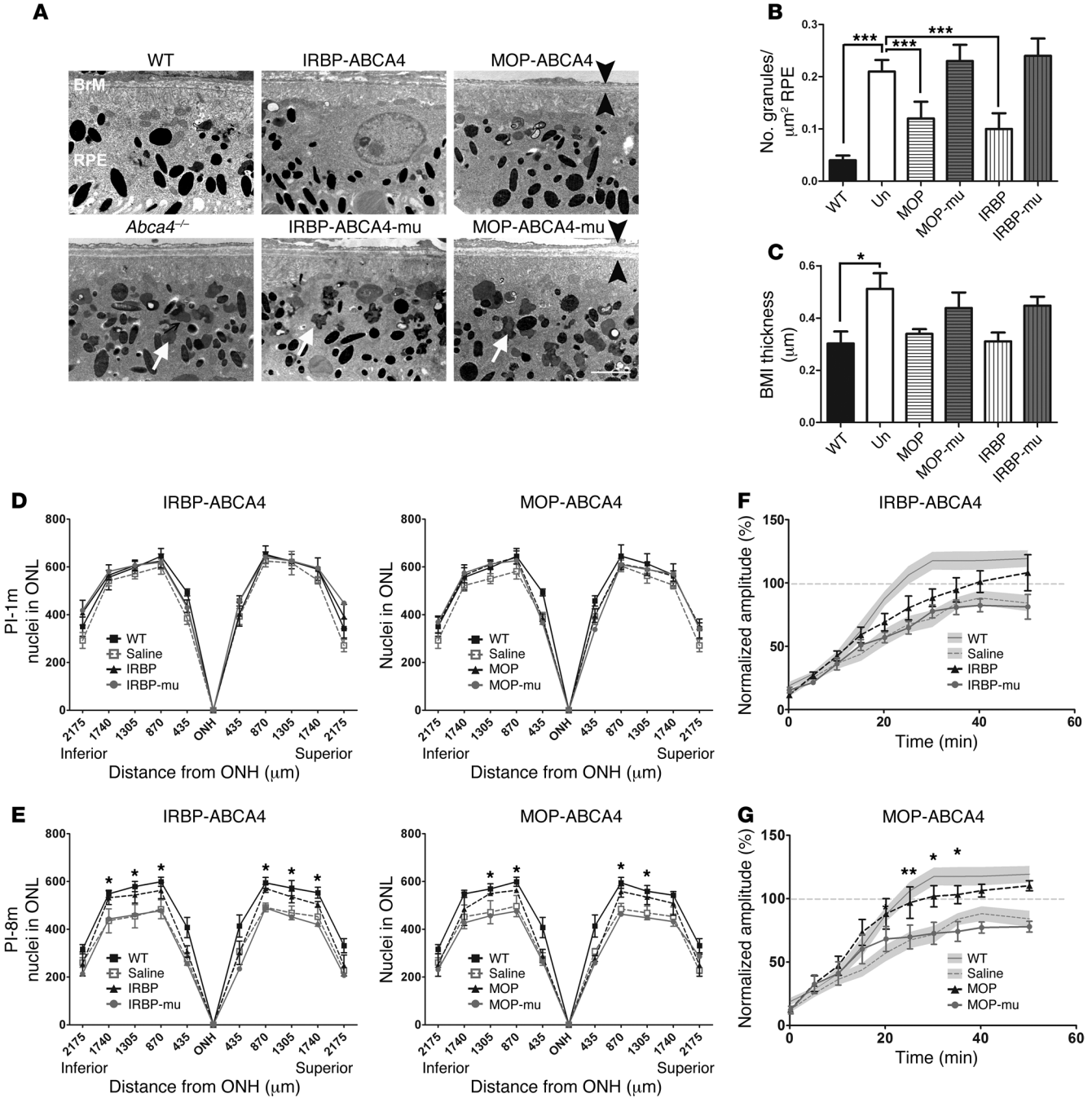

Figure 3

NP-mediated *ABCA4* delivery promotes structural and functional improvement in *Abca4*$^{-/-}$ mice. (**A**) Representative EMs of the RPE layer from animals at 8 months PI. Arrows indicate lipofuscin granules, and arrowheads identify BrM. Scale bar: 2 μm. (**B**) Lipofuscin granules were counted in the RPE by a blinded observer, and results from 3–5 eyes/group are expressed as a function of RPE area analyzed. (**C**) Average BrM (3–5 animals/group). *$P < 0.05$; ***$P < 0.001$ by 1-way ANOVA with Bonferroni's post-hoc tests. The number of nuclei in the ONL in a ×20 field was counted along the vertical meridian at 1 month PI (**D**) and 8 months PI (**E**); ($n = 5$/group). *$P < 0.05$ for comparisons between NP-MOP/IRBP-ABCA4 and NP-MOP-ABCA4-mu/IRBP-ABCA4-mu by 2-way ANOVA. (**F** and **G**) Scotopic ERGs were recorded from dark-adapted WT and *Abca4*$^{-/-}$ mice before and every 5 minutes after a 5-minute (400 lux) photobleach. Mean a-wave amplitudes ± SEM are shown for IRBP-ABCA4/IRBP-ABCA4-mu (**F**), MOP-ABCA4/MOP-ABCA4-mu (**G**), WT (solid line, shaded in gray), and saline (dashed line, shaded in gray). *$P < 0.05$; **$P < 0.01$ by repeated-measures 2-way ANOVA with Bonferroni's post-hoc tests. $n = 4$–10/group.

1 month PI (Figure 3D). In contrast, by 8 months PI (when mice are 9 months old), the number of cells in the central ONL in saline-injected *Abca4*$^{-/-}$ mice was significantly decreased compared with that in WT (Figure 3E). This degeneration was prevented by the ABCA4 NPs. The number of nuclei in the central retina of IRBP-ABCA4 and MOP-ABCA4 mice was significantly improved from saline injected and not significantly different from WT mice. No improvement was noted with mu-NPs. Morphometric results from uninjected animals were not different from those of saline-treated animals (not shown). Combined, these findings indicate that persistent, NP-driven ABCA4 expression at levels between 10% and 25% of WT mediates long-term structural improvement in the *Abca4*$^{-/-}$ mouse.

We next assessed the ability of ABCA4 NPs to mediate functional recovery in *Abca4*$^{-/-}$ mice. The rate of recovery of rod a-wave amplitude at 8 months PI was assessed in NP-treated and age-matched controls. Dark-adapted electroretinogram (ERG) a-waves were measured at baseline and after photobleach every 5 minutes for 50 minutes. No significant differences in prebleach amplitudes were observed for any group, indicating that there were no long-term negative effects of subretinal injections or NP delivery. We observed the expected slowing in the rate of dark adaptation in saline-injected (Figure 3, F and G) and uninjected eyes (not shown) compared with WT. IRBP-ABCA4 NP–treated eyes showed higher mean amplitudes than saline-treated eyes beginning 15 minutes after photobleach, although the differences were not statistically significant. In contrast, a-wave amplitudes in MOP-ABCA4 NP–treated eyes were improved significantly compared with saline-treated eyes. Strikingly, the MOP-ABCA4 NPs achieved WT levels of rescue: at no time after photobleach were means significantly different between MOP-ABCA4–treated animals and WT animals. No improvement in recovery of dark adaptation was observed in IRBP-ABCA4-mu or MOP-ABCA4-mu mice.

Recovery to 100% of prebleach levels was not achieved during the testing period for the majority of uninjected, saline-injected, MOP-ABCA4-mu, or IRBP-ABCA4-mu animals (Supplemental Table 1). In contrast, WT and MOP-ABCA4–treated animals exhibited full recovery in 26.5 ± 3.2 and 27.3 ± 7.7 minutes, respectively (Supplemental Table 1, difference not significant), indicating that MOP-ABCA4 NPs provide virtually complete correction of delayed dark adaptation in the *Abca4*$^{-/-}$ model. Of animals injected with IRBP-ABCA4, 3 out of 6 exhibited full recovery. These data show differential functional rescue with the 2 promoters, although both mediated similar levels of structural improvement. This difference may be due to the rod-based origin of the delayed dark-adaptation phenotype and the fact that the MOP promoter drives expression primarily (2, 17) in rods. While this might suggest that the MOP promoter is the optimal choice for clinical studies, central vision loss is a key patient phenotype and is associated with cone defects (subsequent to RPE damage). *ABCA4*-associated central vision loss is not mimicked in the current mouse model, making it difficult to determine the best promoter for targeting this phenotype in patients.

There remains a great need to develop effective, large capacity delivery tools. Here, we have successfully created NP-based vectors to deliver *ABCA4* and show persistent elevated gene expression that mediates rescue of structural and functional *ABCA4*-associated disease phenotypes. Our DNA NPs offer several advantages, notably safe (1, 6), efficient, persistent expression of large therapeutic genes after subretinal delivery. These widely applicable results suggest that DNA NP–mediated gene delivery can successfully target difficult-to-treat ocular and nonocular genetic diseases, including the many diseases caused by mutations in large genes.

Methods

Generation of DNA NPs. CK30PEG DNA NPs were formulated and verified as described (3). The episomal pEPI-CMV-EGFP vector was provided by Hans J. Lipps (University Witten/Herdecke, Witten, Germany), and WT/mutant (K969M) human *ABCA4* cDNA was provided by Hui Sun (UCLA, Los Angeles, California, USA); see Supplemental Figure 1.

Animal husbandry and subretinal injections. Abca4$^{-/-}$ (Gabriel Travis, Jules Stein Eye Institute, Los Angeles, California, USA) and WT mice on a C57BL/6 background (L450 *Rpe65* variant) were maintained under cyclic light (30 lux, 12L:12D). Subretinal injections were performed at 1 month PI as described (1).

qRT-PCR. qRT-PCR was performed as described (1, 2). Samples were analyzed in triplicate using primers against *ABCA4* (human and mouse) and β-actin. Relative gene expression was determined by ΔCt = (*ABCA4* Ct–β-actin Ct).

Immunofluorescence labeling and Western blotting. Tissue fixation, immunofluorescence, and Western blotting were performed as described (1, 2). Antibodies were anti–ABCA4 3F4 (Robert Molday, University of British Columbia, Vancouver, British Columbia, Canada), goat anti–S-opsin (Santa Cruz Biotechnology Inc.), or anti–β-actin–HRP (Sigma-Aldrich). Imaging was performed using a spinning disk confocal microscope (BX62 Olympus). Blots were imaged and densitometrically analyzed using a Kodak ImageStation 4000r.

Light and electron microscopy, morphometric analysis, and fundus imaging. Eyes were enucleated, fixed, and sectioned as described previously (2). Sections of 0.75 μm containing the optic nerve head were used for morphometry. Cells in a 435-μm section of ONL (×20 image) were counted at intervals from the optic nerve head. Poststained ultrathin sections along the nasal/temporal plane were imaged using a JEOL 100CX electron microscope. Lipofuscin granules were counted manually, and NIH ImageJ was used to determine the BrM thickness and the area of RPE analyzed. Five images per eye were evaluated and summed for each eye. Fundus imaging was conducted using the Micron III (Phoenix Research Labs) as described (18).

ERG analysis. Full-field scotopic ERG was performed on anesthetized mice at 8 months PI after overnight dark adaption using the UTAS system (LKC) (1, 2). Baseline ERG was recorded after a single strobe flash at 1.886 log cd s m^{-2}. Subsequently, animals were exposed to white light (400 lux for 5 minutes). After this photobleach, mice were returned to darkness and ERGs were recorded every 5 minutes.

Statistics. One-way or 2-way ANOVA with Bonferroni's post-hoc comparisons was used as indicated in the legends. All tests were 2-tailed, and significance was defined as $P < 0.05$. Data in figures are plotted as mean ± SEM.

Study approval. All animal experiments were approved by the University of Oklahoma Health Sciences Center Institutional Animal Care and Use Committee and conformed to the *Guide for the Care and Use of Laboratory Animals* (NIH. Revised 2011).

Acknowledgments

The authors thank Barb Nagel, Neal Peachey, and Muayyad Al-Ubaidi for technical assistance, and Gabriel Travis, Hui Sun, and Robert Molday for the *Abca4*$^{-/-}$ mice, *ABCA4* constructs, and ABCA4 antibody, respectively. Financial support was from the National Eye Institute, the Foundation Fighting Blindness, the

Ohio Biomedical Research Commercialization Program, and the Oklahoma Center for the Advancement of Science and Technology.

Received for publication May 15, 2012, and accepted in revised form July 12, 2012.

Address correspondence to: Muna I. Naash, University of Oklahoma Health Sciences Center, Department of Cell Biology, BMSB 781, 940 Stanton L. Young Blvd., Oklahoma City, Oklahoma 73104, USA. Phone: 405.271.8001, ext. 47969; Fax: 405.271.3548; E-mail: Muna-naash@ouhsc.edu.

1. Cai X, Conley SM, Nash Z, Fliesler SJ, Cooper MJ, Naash MI. Gene delivery to mitotic and postmitotic photoreceptors via compacted DNA nanoparticles results in improved phenotype in a mouse model of retinitis pigmentosa. *FASEB J*. 2010;24(4):1178–1191.
2. Cai X, Nash Z, Conley SM, Fliesler SJ, Cooper MJ, Naash MI. A partial structural and functional rescue of a retinitis pigmentosa model with compacted DNA nanoparticles. *PLoS One*. 2009;4(4):e5290.
3. Liu G, et al. Nanoparticles of compacted DNA transfect postmitotic cells. *J Biol Chem*. 2003; 278(35):32578–32586.
4. Ziady AG, et al. Transfection of airway epithelium by stable PEGylated poly-L-lysine DNA nanoparticles in vivo. *Mol Ther*. 2003;8(6):936–947.
5. Ziady AG, et al. Minimal toxicity of stabilized compacted DNA nanoparticles in the murine lung. *Mol Ther*. 2003;8(6):948–956.
6. Han Z, Koirala A, Makkia R, Cooper MJ, Naash MI. Direct gene transfer with compacted DNA nanoparticles in retinal pigment epithelial cells: expression, repeat delivery and lack of toxicity. *Nanomedicine (Lond)*. 2012;4(4):521–539.
7. Yurek DM, et al. Long-term transgene expression in the central nervous system using DNA nanoparticles. *Mol Ther*. 2009;17(4):641–650.
8. Konstan MW, et al. Compacted DNA nanoparticles administered to the nasal mucosa of cystic fibrosis subjects are safe and demonstrate partial to complete cystic fibrosis transmembrane regulator reconstitution. *Hum Gene Ther*. 2004;15(12):1255–1269.
9. Yurek DM, Flectcher AM, Kowalczyk TH, Padegimas L, Cooper MJ. Compacted DNA nanoparticle gene transfer of GDNF to the rat striatum enhances the survival of grafted fetal dopamine neurons. *Cell Transplant*. 2009;18(10):1183–1196.
10. Fink TL, et al. Plasmid size up to 20 kbp does not limit effective in vivo lung gene transfer using compacted DNA nanoparticles. *Gene Ther*. 2006; 13(13):1048–1051.
11. Molday RS. ATP-binding cassette transporter ABCA4: molecular properties and role in vision and macular degeneration. *J Bioenerg Biomembr*. 2007; 39(5-6):507–517.
12. Allocca M, et al. Serotype-dependent packaging of large genes in adeno-associated viral vectors results in effective gene delivery in mice. *J Clin Invest*. 2008; 118(5):1955–1964.
13. Hirsch ML, Agbandje-McKenna M, Samulski RJ. Little vector, big gene transduction: fragmented genome reassembly of adeno-associated virus. *Mol Ther*. 2010;18(1):6–8.
14. Kong J, et al. Correction of the disease phenotype in the mouse model of Stargardt disease by lentiviral gene therapy. *Gene Ther*. 2008;15(19):1311–1320.
15. Weng J, Mata NL, Azarian SM, Tzekov RT, Birch DG, Travis GH. Insights into the function of Rim protein in photoreceptors and etiology of Stargardt's disease from the phenotype in abcr knockout mice. *Cell*. 1999;98(1):13–23.
16. Sun H, Smallwood PM, Nathans J. Biochemical defects in ABCR protein variants associated with human retinopathies. *Nat Genet*. 2000;26(2):242–246.
17. Glushakova LG, et al. Does recombinant adeno-associated virus-vectored proximal region of mouse rhodopsin promoter support only rod-type specific expression in vivo? *Mol Vis*. 2006;12:298–309.
18. Conley SM, Cai X, Makkia R, Wu Y, Sparrow JR, Naash MI. Increased cone sensitivity to ABCA4 deficiency provides insight into macular vision loss in Stargardt's dystrophy. *Biochim Biophys Acta*. 2012;1822(7):1169–1179.
19. Wu L, Nagasaki T, Sparrow JR. Photoreceptor cell degeneration in Abcr (–/–) mice. *Adv Exp Med Biol*. 2010;664:533–539.